http://dx.doi.org/10.1595/147106714X682409 Johnson Matthey Technol. Rev., 2014, 58, (3), 114–123

JOHNSON MATTHEY
TECHNOLOGY REVIEW

www.technology.matthey.com

Comparative Investigations on Platinum Cluster Salts

Experimental characterisation of platinum carbonyl cluster salts for applications in molecular electronics

By Giulia P. M. Bignami*, Alessandro Ceriotti, Patrizia R. Mussini and Cesare Oliva
University of Milan, Via Golgi 19, 20133 Milan, Italy

***Email:** gpm.bignami@gmail.com

Giuliano Longoni and Stefano Zacchini
University of Bologna, Viale Risorgimento 4, 40136 Bologna, Italy

Mattia Gaboardi, Marcello Mazzani and Mauro Riccò
University of Parma, Viale Usberti 7/A, 43124 Parma, Italy

To evaluate future applications of metallic clusters in nanoscience and nanotechnology, the electronic properties of the high-nuclearity carbonyl anionic platinum cluster $[Pt_{19}(CO)_{22}]^{4-}$ were investigated using two different organic cations. In particular, *N,N′*-diethyl viologen dication (Vio^{2+}) and *N,N′*-dimethyl-9,9′-bis-acridinium dication (Acr^{2+}) were employed as counterions, oxidising agents and characterisation probes. The reactions of $[Pt_{19}(CO)_{22}]^{4-}$ tetra-*n*-butylammonium salt, $(TBA^+)_4([Pt_{19}(CO)_{22}]^{4-})$, with both ($Vio^{2+}$) and ($Acr^{2+}$), used as tetraphenylborate salts, yielded two new compounds, which were isolated. The stoichiometries and properties of these new compounds were determined and compared on the basis of infrared (IR) solution spectra, electron spin resonance (ESR) analyses, fluorometric spectra, superconducting quantum interference device (SQUID) magnetometry and resistivity measurements. For Vio^{2+}, a cation-exchange reaction produced the final compound $(Vio^{2+})_2([Pt_{19}(CO)_{22}]^{4-})$, 'PtVio', which was structurally characterised by single crystal X-ray diffraction (XRD) analysis. However, when using Acr^{2+}, a spontaneous redox reaction occurred and a $(Acr^+)(TBA^+)_2([Pt_{19}(CO)_{22}]^{3-})$ stoichiometry for the precipitated solid, 'PtAcr', was inferred from the experimental evidence, leading to an interesting 'doubly-radicalic salt'. This new type of salt, consisting of a radical anionic Pt cluster and a radical cation, is characterised by extremely simple synthesis and isolation processes and by the lowest solid-state resistivity found in high-nuclearity cluster salts with redox-active cations (1).

Introduction

Large metal carbonyl clusters are well-known compounds resembling fragments of metal aggregates stabilised by surrounding carbon monoxide ligands and free negative charges. A recent review reports the synthesis and characterisation of nanosized homo- and heterometallic Pt carbonyl clusters up to 38 and 165 metal atoms respectively (2). Carbonyl clusters are excellent models for the metallic state because their molecular structures mimic very well either bulk metal packings (i.e. cubic close-packed (ccp), hexagonal close-packed (hcp)) or quasicrystalline phases in amorphous metals (i.e. Bagley's pentagonal packing (3)) and can be considered as useful tools to study metallic physical properties, such as electrical conductivity and magnetic behaviour. Electron-transfer processes

involving high-nuclearity metal carbonyl clusters have been investigated (4) as they have a number of potential applications in nanoscience and nanotechnology (5).

Electrochemical research is particularly focusing on high-nuclearity Pt carbonyl clusters, such as $[Pt_{19}(CO)_{22}]^{4-}$ and $[Pt_{24}(CO)_{30}]^{2-}$, which behave as molecular charge capacitors, showing several redox waves with features of electrochemical reversibility (4). This multivalence in redox activity could be exploited to obtain electron-transfer materials based on salts of redox-active anionic clusters and redox-active organic counterions. So far, the only reported examples encompass heterometallic low-nuclearity carbonyl clusters, which are characterised by less developed electrochemical properties and multivalence than high-nuclearity clusters (1). Interestingly, in those cases, an order-of-magnitude decrease was observed in the solid-state cluster salts' resistivity when passing from non redox-active cations to the redox-active *N,N′*-diethyl viologen. In order to better understand the chemistry of such compounds and explore their potential exploitations, the present article reports a comparative study on new cluster salts: a simple exchange-salt and an electron-transfer salt. The latter, in particular, is characterised by the lowest solid-state resistivity found in previously reported electron-transfer cluster salts (1).

Experimental

The compounds were obtained through the spontaneous reaction of the homo-metallic high-nuclearity Pt carbonyl cluster salt $(TBA^+)_4([Pt_{19}(CO)_{22}]^{4-})$ with either *N,N′*-dimethyl-9,9′-bis-acridinium dication (Acr^{2+}) tetraphenylborate salt, $(Acr)(BPh_4)_2$, or *N,N′*-diethyl viologen dication (Vio^{2+}) tetraphenylborate salt, $(Vio)(BPh_4)_2$. These particular organic dications were chosen not only for their redox activity, which played a key role in the synthetic stage, but also for their well-known and widely applied fluorescence, (6–10), in order to have probe molecules through which the nature of the final compounds could be investigated. In particular, Vio is characterised in its dicationic state by a twisted XRD structure (7) and, as density functional theory calculations indicate, it turns planar when the radicalic state is reached (11). In cyclic voltammetry, this dication shows two chemically and electrochemically reversible monoelectronic reduction steps (see the **Supplementary Information** section available on the web version of this article). On the other hand, the Acr structure evolves from twisted to semi-planar when going from its dicationic to its neutral state (6, 8) and its cyclic voltammetry, even if it is affected by such conformational changes, indicates a higher oxidising power than Vio^{2+} (see **Supplementary Information**).

Materials and Reagents

All products and solvents were handled and kept under inert (N_2) atmosphere using Schlenk glassware in order to avoid the possible presence of atmospheric oxygen, which could oxidise and decompose the Pt cluster framework. The classic literature synthesis (12, 13) was performed for the cluster, which can be briefly summarised as follows. Beginning with a Pt wire, a three-step synthesis was carried out, involving:

(a) The dissolution of metallic Pt in *aqua regia*, initially forming hexachloroplatinic acid (H_2PtCl_6) and then sodium hexachloroplatinate (Na_2PtCl_6) by addition of sodium chloride

(b) Reductive carbonylation of Na_2PtCl_6, which was treated with sodium hydroxide under CO atmosphere in methanol solution:

$$9Na_2PtCl_6 + 76NaOH + 37CO \rightarrow (Na^+)_2([Pt_9(CO)_{18}]^{2-}) + 54NaCl + 19Na_2CO_3 + 38H_2O$$

(c) Thermal decomposition – thermal CO evolution in refluxing acetonitrile was used to promote new metal-metal bonds and enlarge the metal nuclearity of the cluster to obtain the final carbonyl cluster $[Pt_{19}(CO)_{22}]^{4-}$:

$$3[Pt_9(CO)_{18}]^{2-} \rightarrow [Pt_{19}(CO)_{22}]^{4-} + [Pt_8(CO)_x]^{2-} + (32-x)CO.$$

The synthetic reactions of $(Vio^{2+})_2([Pt_{19}(CO)_{22}]^{4-})$, PtVio, and $(Acr^+)(TBA^+)_2([Pt_{19}(CO)_{22}]^{3-})$, PtAcr, were performed in acetonitrile (CH_3CN) at room temperature starting from $(TBA^+)_4([Pt_{19}(CO)_{22}]^{4-})$ and either $(Vio)(BPh_4)_2$, obtained from the commercial bromide salt, or $(Acr^{2+})(BPh_4)_2$, obtained from the commercial nitrate salt. In the former case, a 1:2 molar ratio is stoichiometrically required to obtain PtVio precipitation; in the latter case, a 1:1 molar ratio is stoichiometrically required but experimentally a 1:2 molar ratio proved helpful in shifting to the right the precipitation equilibrium of PtAcr.

Instrumentation

IR solution spectra were collected with a Bruker Vector 22 instrument in a calcium fluoride (CaF_2) cell, which was loaded under a constant nitrogen flux.

ESR analyses were performed with a Bruker ELEXSYS E500 instrument both at room temperature, i.e. T = 298 K, and at low temperature, i.e. T = 77 K. The microwave frequency used was 9.7999 GHz for spectra recorded at room temperature and 9.4756 GHz for spectra recorded at low temperature. The power of the microwaves used was 6.3 mW and, when dealing with low temperature analyses, two different types of gain were used: 40 dB and 60 dB.

Direct current (DC) magnetic susceptibility and magnetisation measurements were performed on powder samples with a Magnetic Property Measurement System (MPMS®) XL-5 SQUID magnetometer. Temperature dependent susceptibility was measured in the range of 2 K–300 K in a field exceeding the saturation magnetisation of ferromagnetic impurities. Field dependent magnetisation was measured within the field range $\mu_0 H = \pm 5$ T. The samples, always handled in inert atmosphere, were sealed in a pre-calibrated quartz vial, whose contribution was cancelled by using the instrument's automatic background subtraction mode. A residual helium pressure of 1 mbar guaranteed a good thermal contact.

Electrical resistivity measurements were carried out under nitrogen in a glove bag with a Keithley 2400 SourceMeter on polycrystalline materials pressed into pellets (with a diameter of 8 mm or 13 mm, thickness *ca.* 1 mm) using a four-point probe.

For PtVio, the XRD analysis was performed on crystals obtained by slow diffusion of isopropyl alcohol into a dimethylformamide (DMF) cluster salt solution. The final structure obtained for PtVio was deposited at the Cambridge Crystallographic Data Centre (CCDC), Cambridge, UK, with deposition number CCDC 951529.

Results and Discussion

Infrared Characterisation

The IR spectrum of PtVio in DMF, **Figure 1(a)**, mainly shows the terminal and bridging carbonyl absorption features of the starting $[Pt_{19}(CO)_{22}]^{4-}$ tetraanion (4) at 2002 cm^{-1}(s), 1930 cm^{-1}(w) and 1801 cm^{-1}(m) with a tiny fraction of oxidised cluster at 2024 cm^{-1} and 1820 cm^{-1}, suggesting that a part of PtVio (hereinafter indicated as PtVio*) underwent an internal redox reaction, thus containing $[Pt_{19}(CO)_{22}]^{3-}$ and Vio^{+}.

The IR spectrum of PtAcr in DMF, **Figure 1(b)**, shows the terminal and bridging carbonyl absorption features of the never before isolated $[Pt_{19}(CO)_{22}]^{3-}$ trianion at 2020 cm^{-1} (s), 1953 cm^{-1}(w) and 1821 cm^{-1}(m) with an expected 20 cm^{-1} shift from $[Pt_{19}(CO)_{22}]^{4-}$ absorption features (4).

Electron Spin Resonance Spectrum of PtVio Sample

The ESR spectrum of PtVio sample is composed of a single V line at $g \cong 2.002$ characterised by a peak-to-peak width ΔH_{pp} = 11.47 G nearly independent of temperature, at least down to 77 K. At room temperature, this line is Lorentzian, **Figure 2(a)**, whereas it becomes slightly asymmetric at 77 K. (The 77 K spectrum is not shown because of its low signal to noise ratio.)

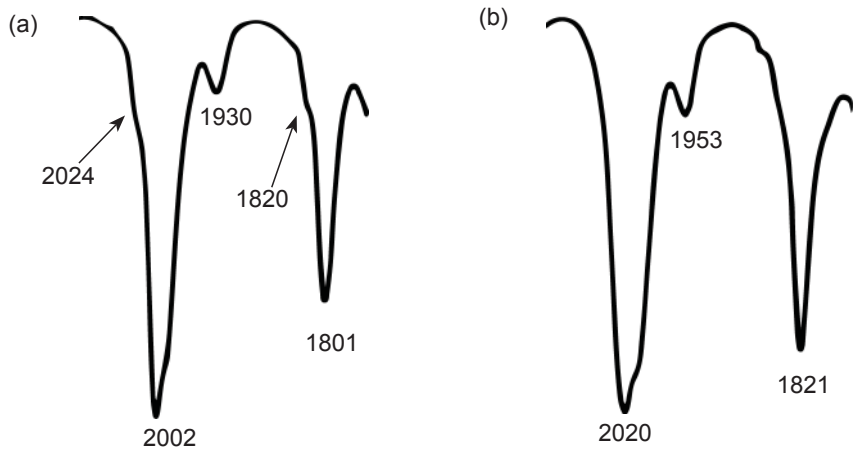

Fig. 1. IR spectra of: (a) PtVio in DMF; and (b) PtAcr in DMF

Electron Spin Resonance Spectrum of PtAcr Sample

The ESR spectrum (not shown here) of the PtAcr sample consists at room temperature of a Lorentzian-shaped A line at g ≅ 2.001 with ΔH_{pp} ≅ 13.50 G. This feature changes somewhat at lower temperature, **Figure 2(b)**, becoming 35% Gaussian- and 65% Lorentzian-shaped and assuming a line width ΔH_{pp} ≅13.20 G at 77 K, whereas a second overlapping ESR pattern B appears, characterised by $g_x \cong g_y \cong 2.03$; $g_z \cong 2.38$ <g> = 2.15 as represented by the calculated red line in **Figure 2(b)**.

Only one paramagnetic species was detected at room temperature with both the PtVio and PtAcr samples, generating in both cases a single ESR line, although this was a bit narrower with the former (V line) than with the latter (A line). The former can be attributed to a Vio^+ monocationic radical, i.e. the organic component of PtVio*. This is similar to that reported in (14) for the cation radical $[Vio^+]_5[Ag_{13}Fe_8(CO)_{32}]^{5-}$·4 DMF. Analogously, the A line, rather similar to V, can be attributed to a Acr^+ monocationic radical. The partially Gaussian shape of A at low temperature can be accounted for by the constrained mobility of the radical species. The B spectrum which is added to the A line of PtAcr at low temperature is attributable to the trianionic odd-electron $[Pt_{19}(CO)_{22}]^{3-\bullet}$. This broad signal is comparable to that reported for the electrogenerated monoanion $[Pt_{24}(CO)_{30}]^{-\bullet}$ at liquid nitrogen temperature (4). That signal was unresolved and displayed a significant spectral anisotropy, attributed to three different g_i parameters, with a mean g value <g> = 2.117, which is only just lower than that of B measured in the present study. Furthermore, the ESR spectrum reported in (4) was rapidly collapsing with increasing temperature, as observed with B, which disappeared at room temperature, though residual traces of it overlapping A cannot be completely excluded in this case.

A rather similar situation is reported in (1), in which $[Fe_3Pt_3(CO)_{15}]^{-\bullet}$ and $[Vio]^{+\bullet}$ in THF solution showed an ESR pattern composed of two overlapping lines with different widths. The $g_x \cong g_y$ values of B are compatible with the $g_\perp$ values of $[Fe_3Pt_3(CO)_{15}]^{-\bullet}$, but the $g_{//}$ value of B is lower than previously reported (15). As a consequence, the <g> ≅ 2.15 mean value found for B in the present study is lower than the <g> ≅ 2.21 reported previously (15). Furthermore, the hyperfine parameter due to the coupling with three Pt atoms was resolved in the previous study, differently from the present case.

Fluorometric Characterisation

Having established (see **Supplementary Information**) that no fluorometric interference could result from the starting cluster, solid-state fluorometric analysis, at a constant excitation wavelength of 366 nm, was carried out on both final compounds, exploiting the known (6–10) fluorescence properties of the two cations used. Unfortunately, this analysis was not helpful for Vio, since its fluorescence properties (7) proved too weak to allow fluorometric characterisation.

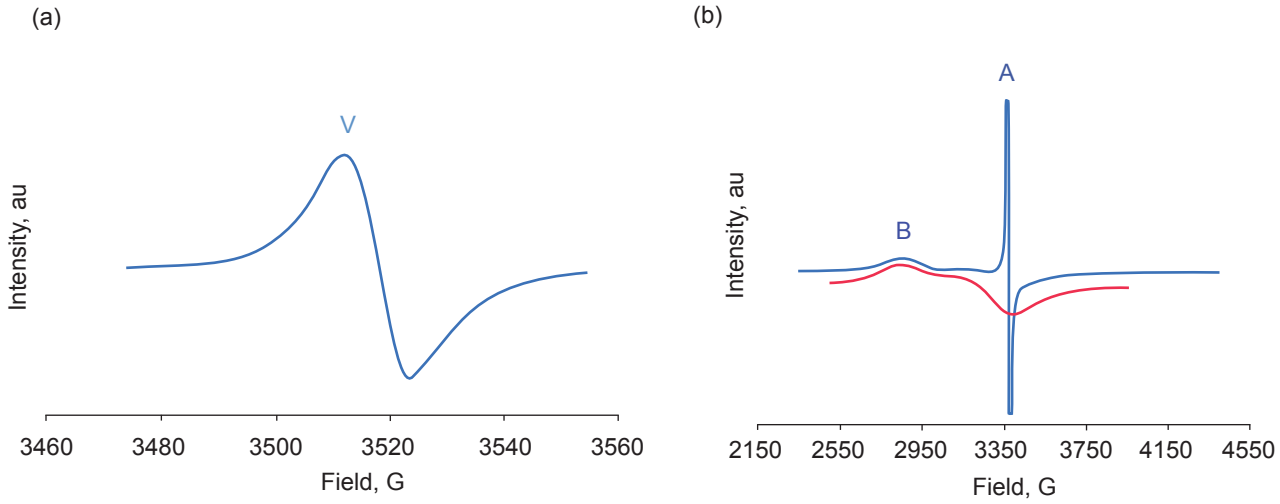

Fig. 2. Solid-state ESR spectra of: (a) PtVio at room temperature, V line: g ≅ 2.002; ΔHpp = 11.47 G; and (b) PtAcr at 77 K, A line: *ca*. 35% Gaussian and 65% Lorentzian; ΔHpp ≅ 13.20 G. Experimental B line: blue; calculated B track: red; <g> = 2.15

The fluorometric emission of Acr was not only much more intense than that of Vio, but was also dependent on the oxidation state of the molecule. Having recorded reference spectra for both its reduced and dicationic oxidised state, it was possible to observe that the fluorometric profile of PtAcr shows the absence of Acr^{2+} fluorometric emission, thus indicating that the final stoichiometry of PtAcr should not include the organic molecule dicationic state (Acr^{2+}).

For a thorough description of the experimental set-up and a more complete report on the final results, see **Supplementary Information**.

Magnetic Analysis

The DC SQUID high-field susceptibility measurements of the PtAcr and PtVio samples in solid-state are shown in **Figure 3**.

The PtAcr susceptibility highlights its paramagnetic nature, as shown by its Curie-like temperature dependence, **Figure 3**. On the one hand, magnetisation curves, M(H), recorded at low temperature clearly indicate that paramagnetism arises from half integer spin states, since the experimental data fit the standard J = ½ Brillouin function (not shown). On the other hand, the temperature dependence of the PtAcr susceptibility allows the microscopic origin of the observed signal to be identified. The least-square analysis, displayed by the blue line in **Figure 3**, was performed according to the Curie-Weiss law (Equation (i)):

$$\chi(T) = \frac{N\mu_B^2 g^2 S(S+1)}{3k_B(T - T_{CW})} + \chi_0 \qquad \text{(i)}$$

(where μ_B is the Bohr magneton and k_B is the Boltzmann constant). ESR measurements have shown a significant contribution to paramagnetism coming from the orbital angular momentum and for this reason the average Landé g-factor g = 2.15 was introduced. The least square analysis, following Equation (i), of the observed susceptibility then gives (assuming S = ½) N = 1.22(2) × 10^{24} spin mol^{-1}. This result is fully consistent with the presence of two spin centres per formula unit ($N \sim 2\ N_{AV}$), namely a spin ½ contribution arises from the odd electron trianionic $[Pt_{19}(CO)_{22}]^{3-}$, while an equivalent spin ½ contribution is given by the organic radical cation.

The room temperature magnetisation curve of bulk PtVio (not shown) displays a weak diamagnetic behaviour (χ_{dia} = −14 ± 1 $mm^3\ mol^{-1}$). Nevertheless, the temperature dependence of its high-field susceptibility exhibits a sizeable paramagnetic fraction, as shown

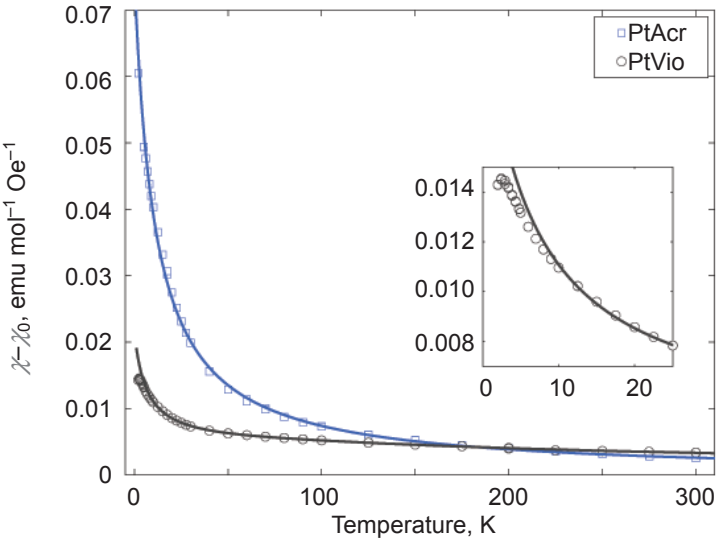

Fig. 3. Temperature dependence of the high field molar susceptibility of PtAcr (blue line, square markers) and PtVio (black line, round markers) samples. A relatively high field (3 T for PtAcr and 0.35 T for PtVio) was applied, in order to saturate the contribution of ferromagnetic impurities. The constant value of χ_0 was subtracted to χ. Inset: zoom of the AFM peak of PtVio, due to the presence of PtVio*

by the black line in **Figure 3**. Such a signal can be mainly attributed to the spin ½, $[Pt_{19}(CO)_{22}]^{3-}$ and Vio^{+}, contributions of PtVio*. This agrees with the detection of partly oxidised clusters by IR spectroscopy and partially reduced cations by ESR spectroscopy. At higher temperatures PtVio susceptibility departs from that of a classical paramagnet: the residual slope of the susceptibility curve is usually a signature of triplet-singlet spin gap thermal excitation.

The data in the range from 9 K to 300 K were fitted to the Bleaney-Bowers equation (Equation (ii)) (16):

$$\chi(T) = A\left[\rho\left(\frac{e^{-\Delta/k_BT}}{1+3e^{-\Delta/k_BT}}\right)+(1-\rho)(T-T_{CW})^{-1}\right]+\chi_0 \qquad \text{(ii)}$$

where $(1-\rho)A = C = N_a\mu_B^2g^2S_a(S_a+1)/3k_B$ is the Curie-Weiss constant of the paramagnet, $\rho A = 2N_b\mu_B^2g^2/3k_B$ is the spin gap fraction and Δ is the exchange integral of the triplet-singlet spin gap. The least square analysis of the data with Equation (ii) reveals that the majority of the sample, i.e. bulk PtVio, is diamagnetic and does not contribute to the magnetic susceptibility (ρ = 0.262(7), N_a~ 0.44 N_{AV} and N_b ~ 0.06 N_{AV}). As anticipated, the main contribution in Equation (ii) (73.8% of the amplitude) is due to the paramagnetic fraction arising from PtVio*. Similarly to the case of PtAcr, PtVio* contributes with two spin S_a = ½ per formula unit, one from $[Pt_{19}(CO)_{22}]^{3-}$ and one from the Vio^{+} counter ion. Hence, from the amplitude of this paramagnetic signal it can be estimated that PtVio* is 22% of the sample. An additional fraction, corresponding to 6% of PtVio, exhibits a triplet-singlet spin gap, which could be ascribed to metal-organic impurities. The transition energy between the triplet fundamental state (S_b = 1) and the singlet excited state (S_b = 0) is Δ = 224.5(1) cm^{-1} (~27.8 meV).

In both systems, the Curie-like paramagnetism presents a negative ordering temperature (T_{CW}) of −11.5(1) K for PtAcr and −6.6 K for PtVio. These negative values are due to antiferromagnetic spin correlations occurring within the paramagnetic phase beneath $|T_{CW}|$. For PtVio, an antiferromagnetic (AFM) transition can be directly observed (see the evident peak at 2.5 K in the inset of **Figure 3**). This is assigned again to PtVio*, whose spin ½ clusters can interact with the unpaired electrons of Vio^{+} cations. Similarly, in the case of PtAcr the AFM correlations are attributed to the exchange interaction between the ½ spin residing on the clusters and the ½ spin of the cations. Moreover, field dependent magnetisation measurements recorded at 300 K (not shown) point out the presence of a tiny ferromagnetic contribution, originating from a small concentration of impurities (approximately equivalent to 25 ppm of iron in both samples), which are commonly found in similar metal clusters (17). The residual temperature-independent susceptibility χ_0 (present in both Equations (i) and (ii)) originates from the sum of these ferromagnetic impurities, diamagnetism and possibly Van Vleck paramagnetism.

Structure and Stoichiometries

All of the obtained data suggest that PtVio bulk stoichiometry can be expressed as $(Vio^{2+})_2([Pt_{19}(CO)_{22}]^{4-})$. Moreover, the XRD structure of this compound, **Figure 4(a)**, was determined using crystals obtained by slow diffusion of isopropanol into a PtVio DMF solution. The $(Vio^{2+})_2([Pt_{19}(CO)_{22}]^{4-})$ elemental cell, see **Figure 4(a)**, contains four cluster units and eight cation molecules, confirming the anion-to-cation stoichiometric ratio. Small differences in the dihedral angles formed by viologen organic rings can be attributed to solid-state packing steric factors rather than intrinsic electronic ones (11). The $[Pt_{19}(CO)_{22}]^{4-}$ structure has an idealised D_{5h} symmetry, consisting of three five-membered rings stacked in an eclipsed conformation with the other four Pt atoms lying on the fivefold axis, two internally sandwiched between the rings and two externally capping the outer pentagonal units. The metal core is surrounded by only 12 terminal COs and 10 edge-bridging COs between the stacked rings, a very small number of protecting carbonyl ligands per surfacial metal atom (CO-to-metal ratio of 1.29) (13).

It was not possible to obtain a crystal structure for PtAcr, notwithstanding several experimental attempts made using a wide variety of crystallisation solvents. However, the combined characterisation results converge to one most plausible stoichiometry that can be formulated as $(Acr^{+})(TBA^{+})_2([Pt_{19}(CO)_{22}]^{3-})$, a salt consisting of a radicalic organic molecule and an odd-electron cluster, resulting from an electron-transfer synthetic path, **Figure 4(b)**. Indeed, this is the only stoichiometry compatible with the composition of the reaction mixture, considering that the trianionic state of the starting cluster is clearly evident from the IR spectra reported, that the absence of Acr^{2+} can be inferred from fluorometric data and that the presence and identity of two radicalic species was shown in ESR spectra and quantified on the basis of SQUID results.

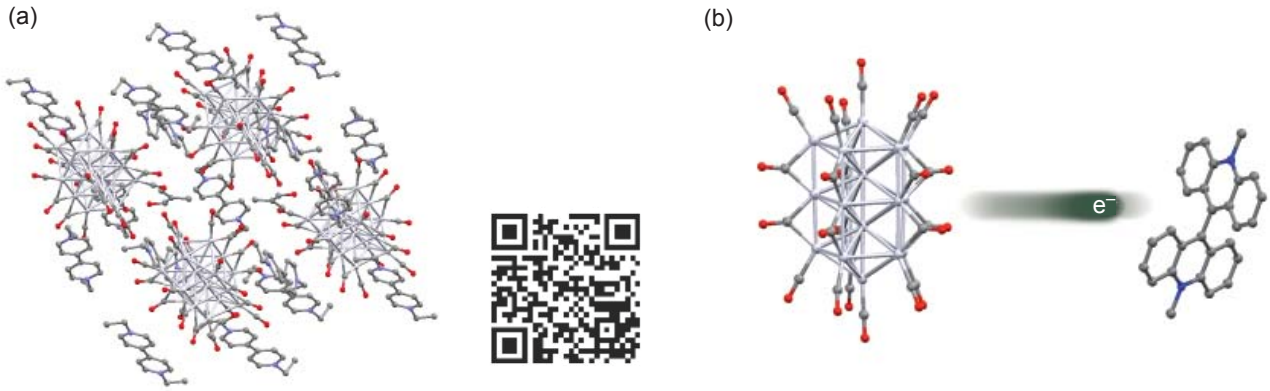

Fig. 4. (a) $(Vio^{2+})_2([Pt_{19}(VO)_{22}]^{4-})$ CCDC 951529 elemental cell; for a three-dimensional visualisation of the structure, see the quick response (QR) code on the right; (b) schematic mono-electronic transfer representation showing $[Pt_{19}(CO)_{22}]^{4-}$ on the left side and Acr^{2+} on the right side. For this compound no crystal structure was obtained probably because of the instability due to its intrinsic doubly-radicalic nature

Resistivity Measurements

The PtAcr data show a perfect linear correlation in a wide current range with a final resistivity value $\rho = 2.3 \times 10^3$ Ωcm, **Figure 5(b)**. On the other hand, **Figure 5(a)** shows that PtVio data keep a linear correlation in a narrower current range, as a result of the higher resistivity of PtVio, $\rho = 1.47 \times 10^6$ Ωcm, compared to that of PtAcr.

The three-order-of-magnitude difference in the solid-state resistivity values of the PtAcr and PtVio compounds observed in this present study is currently under investigation. It is thought to be related to the presence of radicalic redox-active centres in the PtAcr sample, in contrast to the closed-shell redox-active centres found in the PtVio sample. The possible influence of structural powder factors, as suggested by scanning electron microscope (SEM) images (see the **Supplementary Information**), should also be considered, since electrical measurements have been performed on pressed polycrystalline pellets.

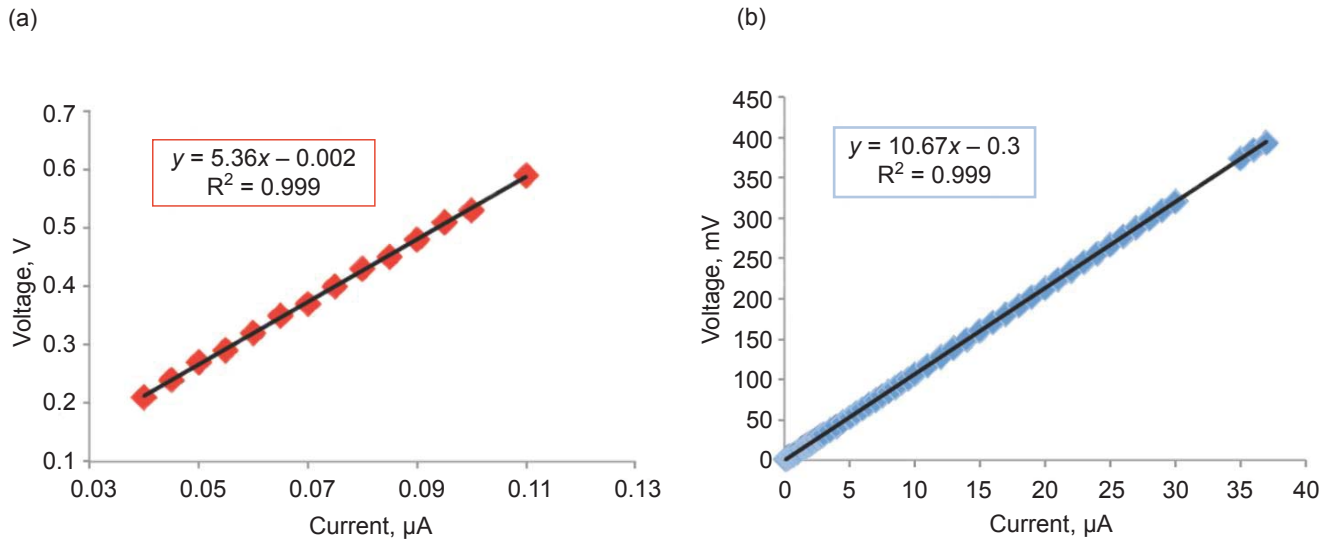

Fig. 5. (a) PtVio V/Volt vs. I/μA plot; (b) PtAcr V/Volt vs. I/μA plot. In both cases, the final resistivity values were obtained from the slopes of the linear fits to the experimental points

Furthermore, interestingly, the extremely low resistivity value obtained for PtAcr can be compared to the reported values of intrinsic semiconductors such as silicon or germanium and has been previously reached, in the case of Pt carbonyl clusters, only when Pt frameworks self-assemble into infinite wires upon crystallisation (18, 19).

Conclusions

In conclusion, it has been shown that high-nuclearity Pt cluster salts, in combination with organic redox-active cations, should be considered as promising materials for future applications in molecular electronics. In particular, when using Vio^{2+}, the final compound, $(Vio^{2+})_2([Pt_{19}(CO)_{22}]^{4-})$, exhibited an exchange-salt stoichiometry. In such a doubly-closed-shell salt, the incipient redox activity of both the cluster and the cation, as indicated by the experimental results obtained in this study, together with the stability of the starting system, could be exploited to prepare doubly-radicalic species, such as $(Vio^{+})(Vio^{2+})([Pt_{19}(CO)_{22}]^{3-})$, *via* controlled photochemical, chemical or thermal post-synthesis inductions.

On the other hand, when using Acr^{2+}, as a result of its higher oxidising power, a spontaneous redox reaction occurred and a reasonable $(Acr^{+})(TBA^{+})_2([Pt_{19}(CO)_{22}]^{3-})$ stoichiometry for the precipitated solid was inferred from the available evidence, leading to an interesting fluorescent 'doubly-radicalic salt'. This type of salt, isolated and fully characterised here for the first time and consisting of a radical anionic Pt cluster and a fluorescent radical cation, was obtained by an extremely simple synthetic process and shows the lowest solid-state resistivity compared to previously reported cases (1), reaching semiconductor-like values. Therefore, it is possible to conclude that the future development of the new Pt cluster salts described above could break the boundaries of synthetic Pt cluster chemistry, eventually entering the field of materials chemistry.

Acknowledgements

The authors would like to thank Piero Macchi (University of Bern, Switzerland) for the PtVio crystallographic structure determination. Moreover, we would like to thank Monica Panigati, Stefania Righetto and Serena Cappelli (University of Milan, Italy) for their help in acquiring the cyclic voltammetry, fluorometry and electron spin resonance experimental data, respectively.

References

1 C. Femoni, M. C. Iapalucci, G. Longoni, C. Tiozzo, J. Wolowska, S. Zacchini and E. Zazzaroni, *Chem. Eur. J.*, 2007, **13**, (23), 6544

2 I. Ciabatti, C. Femoni, M. C. Iapalucci, G. Longoni and S. Zacchini, *J. Clust. Sci.*, 2014, **25**, (1), 115

3 B. G. Bagley, *Nature*, 1970, **225**, 1040

4 S. Fedi, P. Zanello, F. Laschi, A. Ceriotti and S. El Afefey, *J. Solid State Electrochem.*, 2009, **13**, (10), 1497

5 C. Femoni, M. C. Iapalucci, F. Kaswalder, G. Longoni and S. Zacchini, *Coord. Chem. Rev.*, 2006, **250**, (11–12), 1580

6 E. Ahlberg, O. Hammerich and V. D. Parker, *J. Am. Chem. Soc.*, 1981, **103**, (4), 844

7 P. M. S. Monk, "The Viologens: Physicochemical Properties, Synthesis and Applications of the Salts of 4,4'-Bipyridine", John Wiley & Sons, Chichester, UK, 1998

8 I. Spasojević, S. I. Liochev and I. Fridovich, *Arch. Biochem. Biophys.*, 2000, **373**, (2), 447

9 C. D. Geddes, *Dyes Pigments*, 2000, **45**, (3), 243

10 A. W-H. Mau, J. M. Overbeek, J. W. Loder and W. H. F. Sasse, *J. Chem. Soc., Faraday Trans. 2*, 1986, **82**, (5), 869

11 P. Macchi, Department of Chemistry and Biochemistry, University of Bern, personal communication, 2013

12 G. Longoni and P. Chini, *J. Am. Chem. Soc.*, 1976, **98**, (23), 7225

13 D. M. Washecheck, E. J. Wucherer, L. F. Dahl, A. Ceriotti, G. Longoni, M. Manassero, M. Sansoni and P. Chini, *J. Am. Chem. Soc.*, 1979, **101**, (20), 6110

14 D. Collini, C. Femoni, M. C. Iapalucci and G. Longoni, *Comptes Rendus Chimie*, 2005, **8**, (9–10), 1645

15 G. Longoni and F. Morazzoni, *J. Chem. Soc., Dalton Trans.*, 1981, (8), 1735

16 B. Bleaney and K. D. Bowers, *Proc. R. Soc. Lond. A*, 1952, **214**, (1119), 451

17 C. Femoni, M. C. Iapalucci, G. Longoni, J. Wolowska, S. Zacchini, P. Zanello, S. Fedi, M. Riccò, D. Pontiroli and M. Mazzani, *J. Am. Chem. Soc.*, 2010, **132**, (9), 2919

18 C. Femoni, F. Kaswalder, M. C. Iapalucci, G. Longoni and S. Zacchini, *Eur. J. Inorg. Chem.*, 2007, (11), 1483

19 C. Femoni, M. C. Iapalucci, G. Longoni, T. Lovato, S. Stagni and S. Zacchini, *Inorg. Chem.*, 2010, **49**, (13), 5992

20 G. Casalbore-Miceli, N. Camaioni, A. Geri, G. Ridolfi, A. Zanelli, M. C. Gallazzi, M. Maggini and T. Benincori, *J. Electroanal. Chem.*, 2007, **603**, (2), 227

21 S. Chatterjee, S. Basu, N. Ghosh and M. Chakrabarty, *Chem. Phys. Lett.*, 2004, **388**, (1–3), 79

22 F. Millich and G. Oster, *J. Am. Chem. Soc.*, 1959, **81**, (6), 1357

The Authors

Giulia Bignami graduated in 2013 from the University of Milan with a Master's degree in Chemical Sciences. Her two-year-long research project focused on investigating new synthetic pathways and characterisation processes for platinum cluster salts. She has now moved to the University of St Andrews, UK, where she is currently undertaking a PhD.

Alessandro Ceriotti is Associate Professor of Inorganic Chemistry at the University of Milan, where he lectures coordination chemistry for undergraduate students. He is author of about 80 scientific papers. His major research activity is concerned with the synthesis and characterisation of high-nuclearity metal carbonyl clusters.

Patrizia Romana Mussini is Associate Professor of Analytical Chemistry at the University of Milan. Her expertise in electrochemistry and electroanalysis is accounted for by about 150 peer reviewed scientific papers. She is currently concerned with the application of electroanalytical techniques for characterising and developing advanced molecular materials.

Cesare Oliva is Associate Professor at the University of Milan and Associate to the Italian Consiglio Nazionale delle Ricerche (CNR) Institute of Molecular Sciences and Technologies (ISTM). His research in the electron paramagnetic resonance spectroscopy is documented by *ca*. 120 publications on scientific journals and by several communications at international and national meetings.

Giuliano Longoni received a degree in Industrial Chemistry at the University of Milan in 1967. He became Research Associate of Italian CNR in 1973 and Associate Professor at the University of Milan in 1983. He is Full Professor at the University of Bologna, Italy, since 1986. Formerly a member of the Editorial Board of *Inorganic Chemistry* and *Journal of Cluster Science*, he is author of about 180 scientific papers.

Stefano Zacchini received a degree in Industrial Chemistry at the University of Bologna in 1996 and his PhD in Chemistry at University of Liverpool in 2001. After a post-doctoral fellowship in Liverpool during 2001–2002, he became Research Associate at the University of Bologna and, since 2010, Associate Professor of Inorganic Chemistry.

Mattia Gaboardi received his Master's degree in Material Science in 2010 and his PhD in Physics in 2014 at the University of Parma, studying the synthesis and physical properties of intercalated fullerides for hydrogen storage. He is currently Postdoctoral Researcher in the Carbon Nanostructures group in the Department of Physics and Earth Science at the University of Parma.

Marcello Mazzani received his PhD in Physics in 2011 at the University of Parma, on the electronic and magnetic properties of carbon-based materials for ionic conductivity and hydrogen storage, with a pioneer work for graphene characterisation using ultrasonication route (USR) and neutron scattering. He is currently extending his research interests towards material relevant for energy technologies and environmental science.

Mauro Riccò is Associate Professor in the Department of Physics and Earth Science at the University of Parma since 2004. He coordinates Carbon Nanostructures, a pioneer group for the research on fullerenes. He is the author of 80 scientific papers on international journals and has held 13 invited lectures at international conferences.